Supporting Information

Atomic Bridging Modulation of Ir–N, S co-doped MXene for Accelerating Hydrogen evolution

Wujun Lin[a#], Ying-Rui Lu[b#], Wei Peng[a], Min Luo[c*], Ting-Shan Chan[b*], Yongwen Tan[a*]

[a]College of Materials Science and Engineering, State Key Laboratory of Advanced Design and Manufacturing for Vehicle Body, Hunan University, Changsha, Hunan 410082, China.

[b]National Synchrotron Radiation Research Center, Hsinchu 300, Taiwan.

[c]Shanghai Technical Institute of Electronics & Information, Shanghai 201411, China.

[#]These authors contributed equally to this work.

* Corresponding author.

E-mail: luomin@sspu.edu.cn (Min Luo), chan.ts@nsrrc.org.tw (Ting-Shan Chan), tanyw@hnu.edu.cn (Yongwen Tan)

Experimental section

Synthesis of Catalysts

Preparation of H^+ melamine

2 g melamine was dissolved in 30 mL ethanol under magnetic stirring for 15 minutes. Then, 3 mL of 12 mol L^{-1} hydrochloric acid was slowly added into the mixed solution followed by stirring for 30 minutes. After washing with ethanol and deionized water for several times and centrifugation, H^+ melamine was obtained by dried at 60℃ in a vacuum oven for 10 h.

Synthesis of Ti_3C_2 MXene

$Ti_3C_2T_x$ MXene was synthesized by selective etching of Al layers from Ti_3AlC_2 MAX phase. Typically, 1 g of LiF was dissolved in a mixed solution of 5 mL deionized water and 15 mL HCl with magnetic stirring in a plastic beaker which was put it into ice-bath. After stirring for 15 minutes, 1 g of Ti_3AlC_2 powders were slowly added into the mixed solution at the temperature of 35 ℃. The beaker was then transferred into oil-bath with a constant temperature of 35 ℃. After magnetic stirring for 24h, the mixture was transferred into centrifuge tube and washed with deionized water for several times (3500 rpm, 5 minutes) until the pH value reached 6. Subsequently, the supernatant was decanted to collect the sediment which contained the multilayered $Ti_3C_2T_x$. The delaminated $Ti_3C_2T_x$ flakes were prepared by ultrasonicating the re-dispersed sediment solution for 45 minutes in ice-bath. Meanwhile, argon gas was introduced to prevent oxidation. Finally, the solution was centrifuged at 3500 rpm for 1 h, then collecting the dark supernatant consisting of the

delaminated 2D MXene flakes.

Synthesis of Ir_{SA}-NS-$Ti_3C_2T_x$

3 mL of above collected MXene flakes supernatant (10 mg L^{-1}) and 30 mg of H^+ melamine was dissolved in 10 mL of deionized water. Meanwhile, 60 mg of thiourea was dissolved in 10 ml of deionized water. To synthesize the Ir-2NS-$Ti_3C_2T_x$, the $Ti_3C_2T_x$ supernatant was added into a centrifuge tube. Subsequently, the H^+ melamine solution, H_2IrCl_6 solution, and thiourea solution were quickly added into the $Ti_3C_2T_x$ supernatant and freeze-dried for 72 h. The obtained freeze-dried foam was transferred into the middle of tube furnace and heat at 550 ℃ for 2 h under Argon atmosphere (heating rate: 5 ℃ min^{-1}). Finally, the resultant black powder was collected and named as Ir_{SA}-2NS-$Ti_3C_2T_x$. For comparison, Ir_{SA}-1NS-$Ti_3C_2T_x$, Ir_{SA}-3NS-$Ti_3C_2T_x$, and Ir-N-$Ti_3C_2T_x$ samples were prepared by the same procedure except changing the amount of thiourea; 1, 2 and 3 represents the mass ratio of precursor thiourea and $Ti_3C_2T_x$ MXene is 1:1, 1:2 and 1:3, respectively.

Material characterizations

X-ray diffraction data were obtained through a Bruker D8 Advance X-ray diffractometer with Cu Kα radiation (γ = 1.5418 A). Scanning electron microscopy (Zeiss Sigma HD equipped with an Oxford EDS) and Transmission electron microscopy (JEM-ARM 200F) were performed to characterize the morphology and element distribution map of catalysts. X-ray photoelectron spectroscopy spectra were obtained by Thermo Scientific ESCALAB250Xi spectrometer with Al Kα monochromatic. The loading of Ir in Ir_{SA}-2NS-$Ti_3C_2T_x$ was recorded by Inductively

coupled plasma optical emission spectrometry on Agilent 730. The Ir L_3-edge and S K-edge X-ray absorption spectra were obtained at the beamline 01C1 of National Synchrotron Radiation Research Center (NSRRC, Taiwan) in the fluorescence mode.

DFT calculations

The DFT calculations were conducted using the Vienna ab initio simulation package with the projected projector augmented wave method. The monolayer $Ti_3C_2T_x$ was simulated with the supercell model. The main termination of $Ti_3C_2T_x$ is O, as suggested by the XPS results. Therefore, a (4×4×1) $Ti_3C_2O_2$ cell was employed in DFT calculation. The atomic model of the $Ti_3C_2O_2$ monolayer was shown in **Fig S18**. At the same time, the XPS and XAFS results of Ir_{SA}-2NS-$Ti_3C_2T_x$ shows the formation of Ti-N, Ir-N, S-C, Ir-S, and S-Ti bonds after Ir, N, and S doping, which suggests that some O and C atoms of $Ti_3C_2O_2$ monolayer were replaced by N and S atoms (**Fig S19**). A vacuum region of 18 Å was used for all calculation to eliminate the neighboring cells interactions. All the atoms were optimized until the residual forces were less than 0.01 eV $Å^{-1}$.

The Gibbs free energy of the adsorbed state (ΔG_H) was obtained as follows:

$$\Delta G_H = \Delta E_{H*} + \Delta E_{ZPE} - T\Delta S \qquad \text{(S1)}$$

Where ΔE_{H*} is the hydrogen binding energy, ΔE_{ZPE} is the zero-point energy difference, and ΔS is the entropy change of hydrogen adsorption.

Electrochemical characterizations

Electrochemical HER measurements were performed on an electrochemical workstation (CHI 760E) under ambient conditions. To prepare catalysts' ink, typically,

2 mg of as-prepared catalysts and 10 μL Nafion solution (Alfa Aesar, 5wt%) were dispersed in 490 μL ethanol by sonication for 30min. Geometric area of carbon paper is 0.25 cm^2. Then, 20 μL of catalysts' ink were dropped on the carbon paper and dried in the air. A graphite rod was used as the counter electrode, an Ag/AgCl electrode as the reference electrode, and the catalyst coated carbon paper as the working electrode. Linear sweep voltammetry was performed in Ar saturated 0.5 M H_2SO_4 and 1.0 M KOH solution at a scan rate of 1 mV s^{-1}. All data were *IR* corrected. All potentials were converted to the reversible hydrogen electrode (RHE) according to following equations: [$E_{(RHE)} = E_{(Ag/AgCl)} + 0.059\ pH + 0.197\ V$]. Chronoamperometric characterization data was collected at a potential of 58 mV versus RHE for 38 h.

Note:

Calculation of TOFs for HER

Acidic HER:

$$n = \frac{2 \times 10^{-3} \times 2.5\% \times \frac{20}{500}}{192.22} = 1.04 \times 10^{-8} mol$$

Ir_{SA}-1NS-$Ti_3C_2T_x$:

$$TOF(@0.06V) = \frac{I}{2F \times n} = \frac{0.00073}{2 \times 96500 \times 1.04 \times 10^{-8}} = 0.36\ s^{-1}$$

$$TOF(@0.08V) = \frac{I}{2F \times n} = \frac{0.00116}{2 \times 96500 \times 1.04 \times 10^{-8}} = 0.58\ s^{-1}$$

$$TOF(@0.10V) = \frac{I}{2F \times n} = \frac{0.00204}{2 \times 96500 \times 1.04 \times 10^{-8}} = 1.02\ s^{-1}$$

Ir_{SA}-2NS-~~np~~$Ti_3C_2T_x$:

$$TOF(@0.06V) = \frac{I}{2F \times n} = \frac{0.00291}{2 \times 96500 \times 1.04 \times 10^{-8}} = 1.45\ s^{-1}$$

$$TOF(@0.08V) = \frac{I}{2F \times n} = \frac{0.014}{2 \times 96500 \times 1.04 \times 10^{-8}} = 6.97\ s^{-1}$$

$$TOF(@0.10V) = \frac{I}{2F \times n} = \frac{0.03142}{2 \times 96500 \times 1.04 \times 10^{-8}} = 15.65\ s^{-1}$$

Ir_{SA}-3NS-~~np~~$Ti_3C_2T_x$:

$$TOF(@0.06V) = \frac{I}{2F \times n} = \frac{0.00099}{2 \times 96500 \times 1.04 \times 10^{-8}} = 0.49\ s^{-1}$$

$$TOF(@0.08V) = \frac{I}{2F \times n} = \frac{0.00172}{2 \times 96500 \times 1.04 \times 10^{-8}} = 0.86\ s^{-1}$$

$$TOF(@0.10V) = \frac{I}{2F \times n} = \frac{0.00425}{2 \times 96500 \times 1.04 \times 10^{-8}} = 2.12\ s^{-1}$$

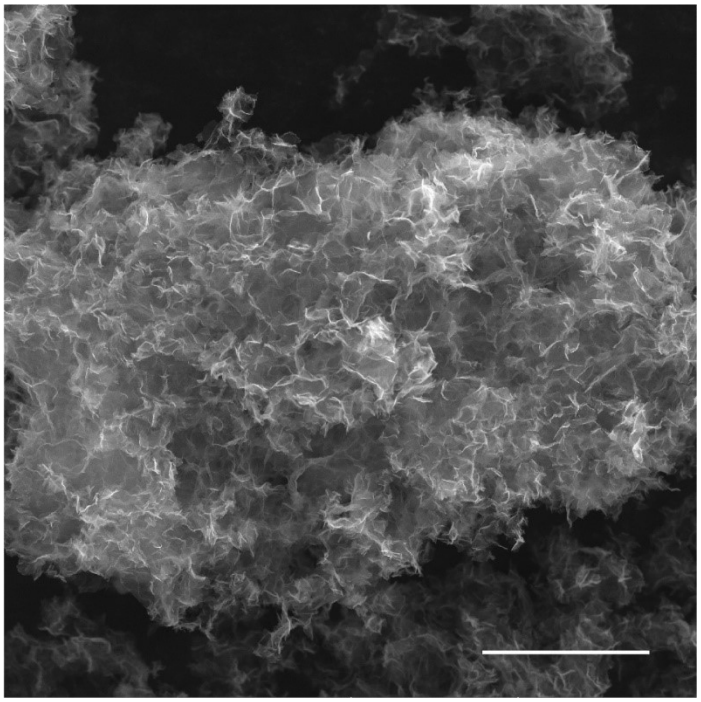

Figure S1. A typical SEM image of the as-prepared 2NS-$Ti_3C_2T_x$. Scale bar: 10 μm.

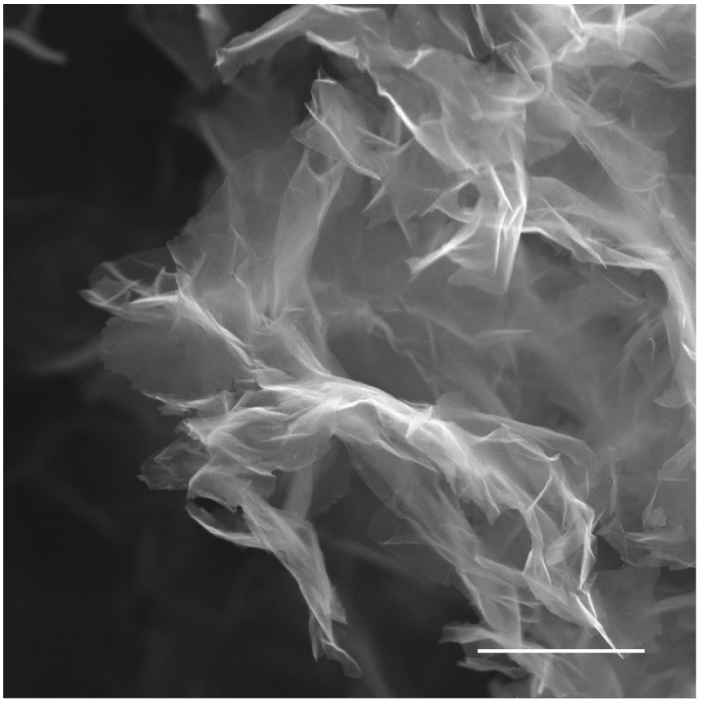

Figure S2. High magnification SEM image of the as-prepared Ir_{SA}-2NS-$Ti_3C_2T_x$.

Scale bar: 1 μm.

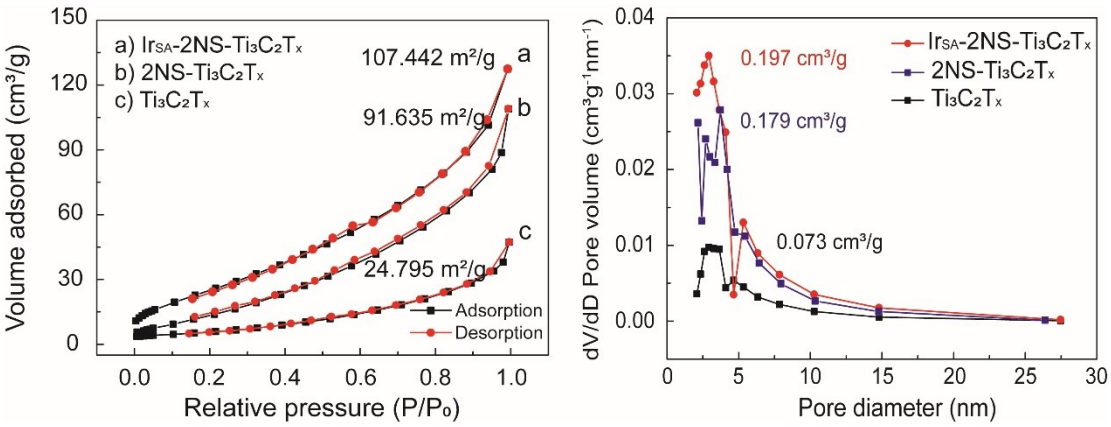

Figure S3. (a) BET curves of the $Ti_3C_2T_x$, 2NS-$Ti_3C_2T_x$ and Ir_{SA}-2NS-$Ti_3C_2T_x$. (b) The pore-size distribution of the $Ti_3C_2T_x$, 2NS-$Ti_3C_2T_x$ and Ir_{SA}-2NS-$Ti_3C_2T_x$.

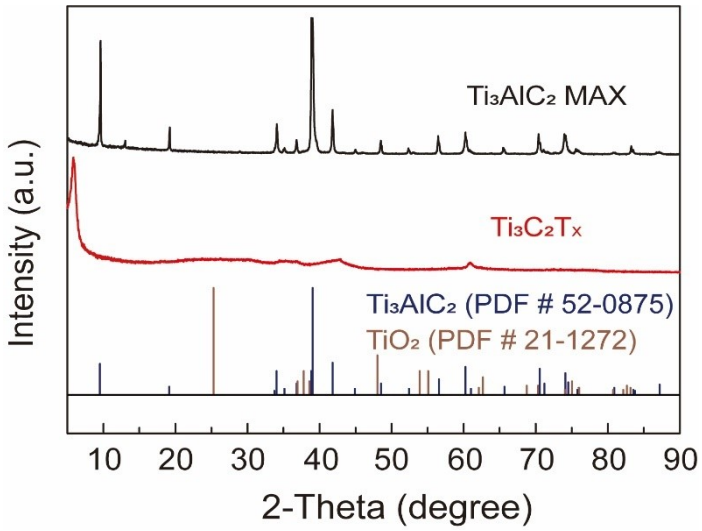

Figure S4. X-ray diffraction patterns of Ti_3AlC_2 MAX and $Ti_3C_2T_x$ MXene.

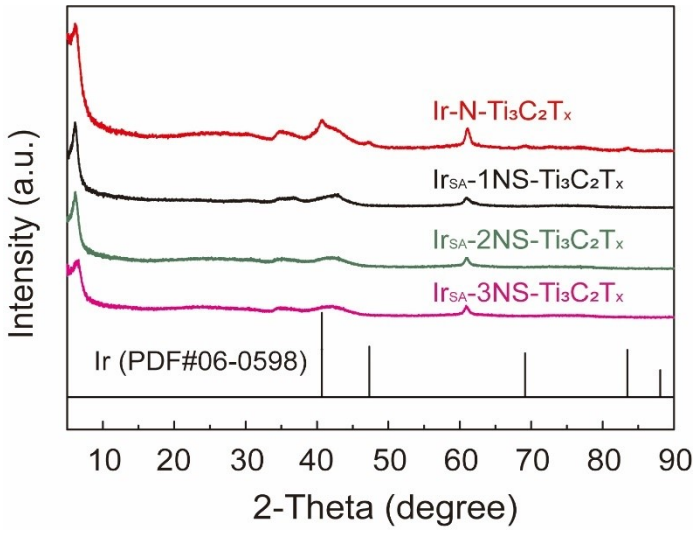

Figure S5. X-ray diffraction patterns of Ir-N-$Ti_3C_2T_x$, Ir_{SA}-1NS-$Ti_3C_2T_x$, Ir_{SA}-2NS-$Ti_3C_2T_x$, and Ir_{SA}-3NS-$Ti_3C_2T_x$.

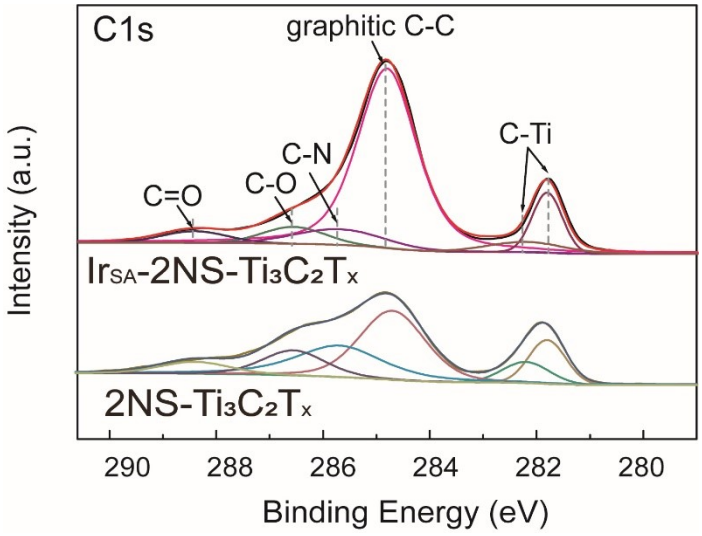

Figure S6. High resolution C 1*s* XPS spectra of the Ir_{SA}-2NS-$Ti_3C_2T_x$ and 2NS-$Ti_3C_2T_x$ catalyst.

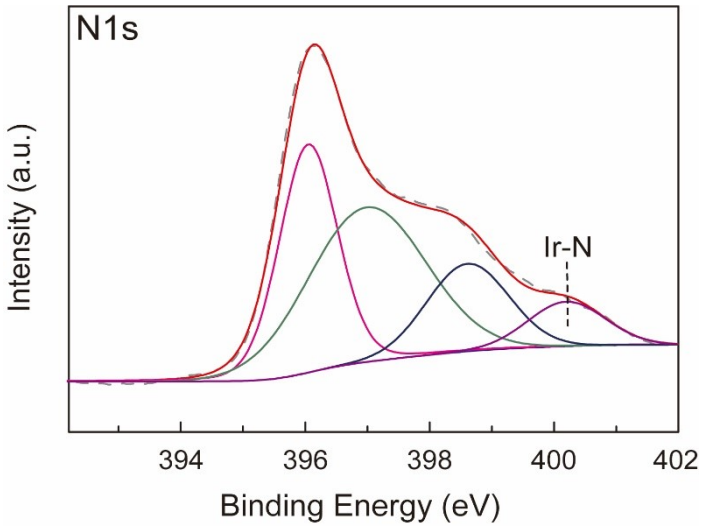

Figure S7. High resolution N 1*s* XPS spectra of the Ir_{SA}-1NS-$Ti_3C_2T_x$ catalyst.

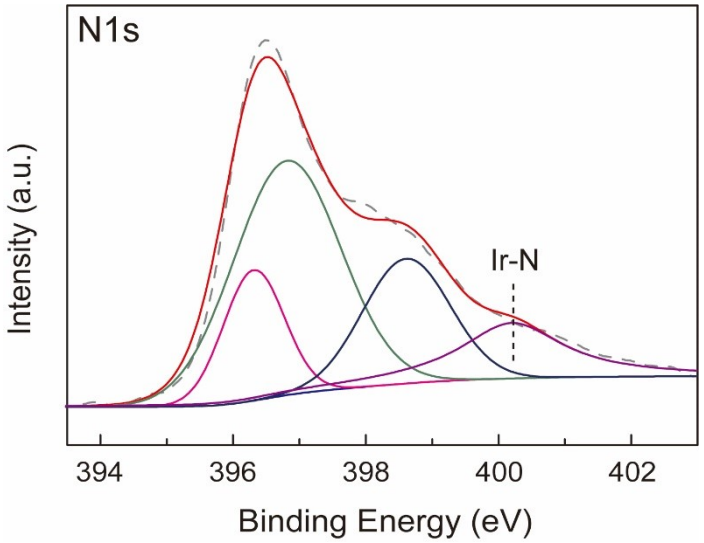

Figure S8. High resolution N 1*s* XPS spectra of the Ir_{SA}-3NS-$Ti_3C_2T_x$ catalyst.

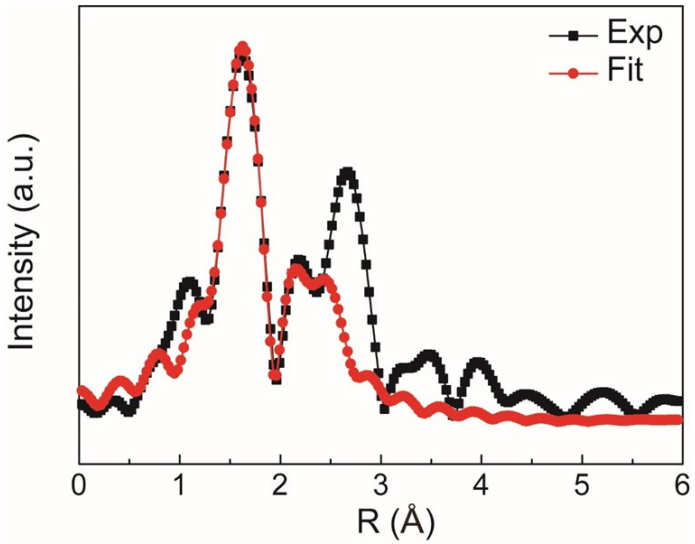

Figure S9. FT-EXAFS fitting curves of Ir_{SA}-2NS-$Ti_3C_2T_x$ catalyst.

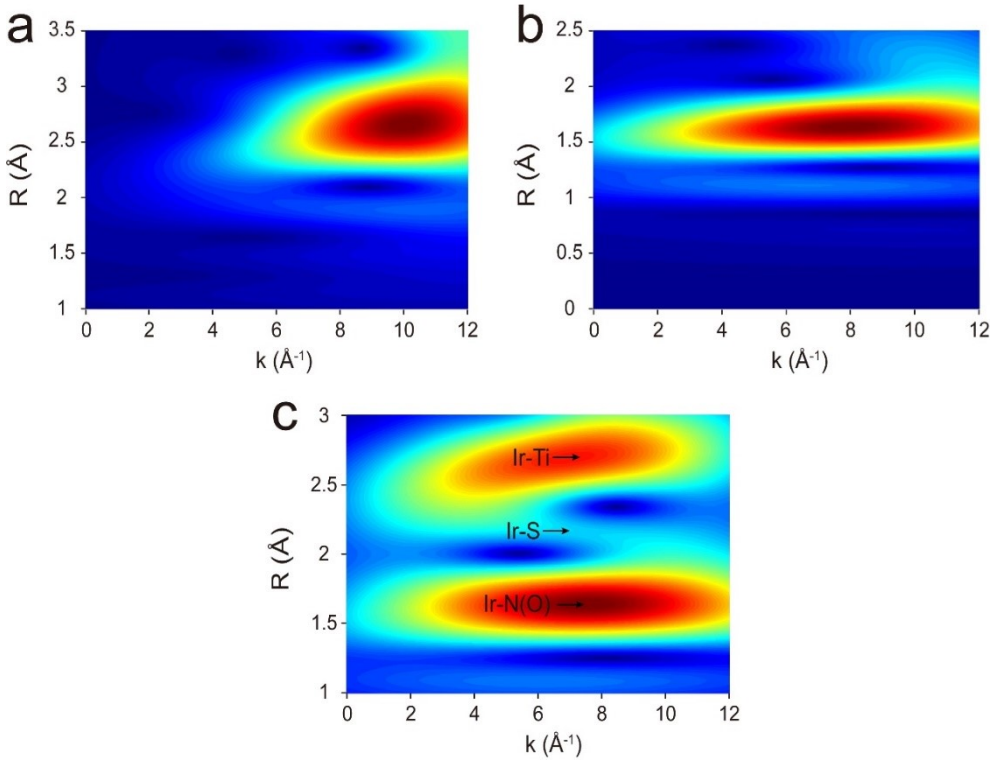

Figure S10. Wavelet transforms (WT) of EXAFS spectra of Ir foil, IrO_2 and Ir_{SA}-2NS-$Ti_3C_2T_x$.

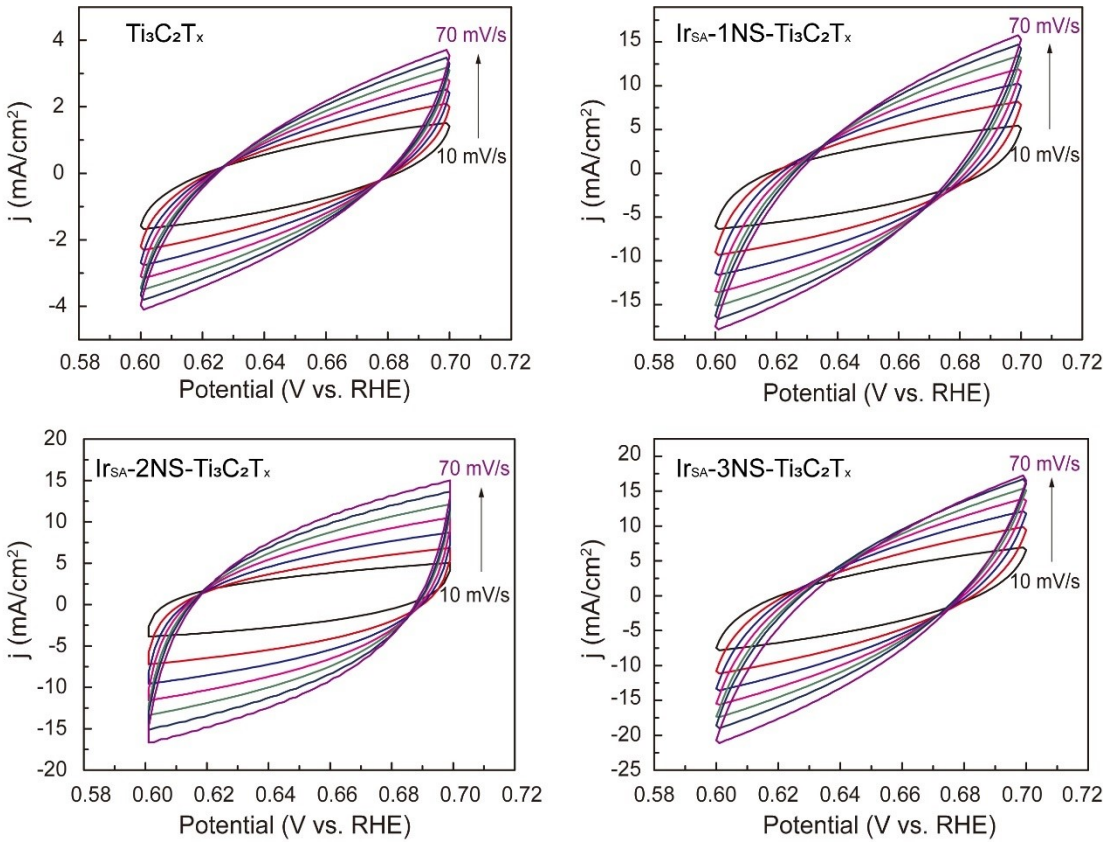

Figure S11. CV curves of $Ti_3C_2T_x$, Ir_{SA}-1NS-$Ti_3C_2T_x$, Ir_{SA}-2NS-$Ti_3C_2T_x$, and Ir_{SA}-3NS-$Ti_3C_2T_x$ at different scan rates in 0.5 M H_2SO_4.

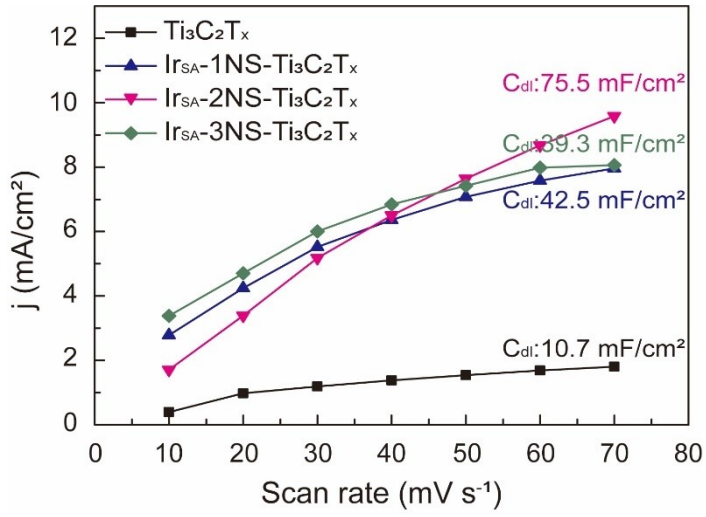

Figure S12. The calculated double-layer capacitance value (C_{dl}) of $Ti_3C_2T_x$, Ir_{SA}-1NS-$Ti_3C_2T_x$, Ir_{SA}-2NS-$Ti_3C_2T_x$, and Ir_{SA}-3NS-$Ti_3C_2T_x$.

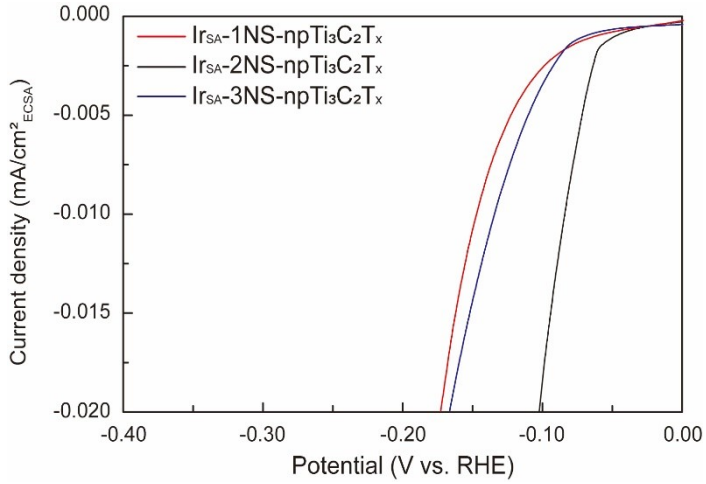

Figure S13. ECSA-normalized LSV curves of Ir_{SA}-1NS-$Ti_3C_2T_x$, Ir_{SA}-2NS-$Ti_3C_2T_x$, and Ir_{SA}-3NS-$Ti_3C_2T_x$.

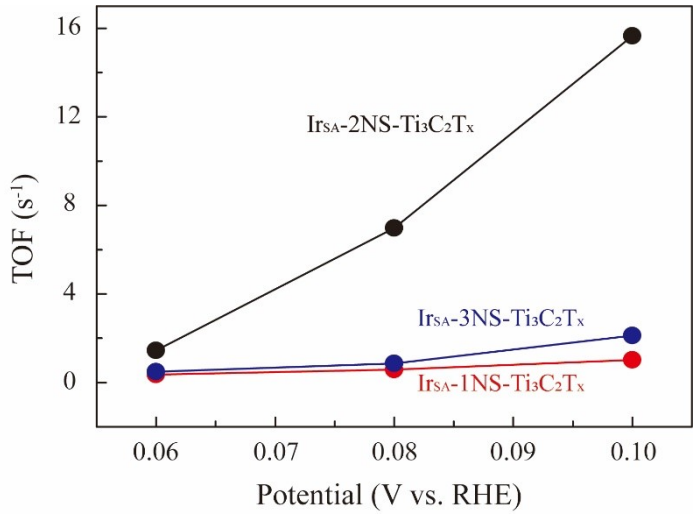

Figure S14. Turnover frequency (TOF) curves of Ir_{SA}-1NS-$Ti_3C_2T_x$, Ir_{SA}-2NS-$Ti_3C_2T_x$, and Ir_{SA}-3NS-$Ti_3C_2T_x$ samples.

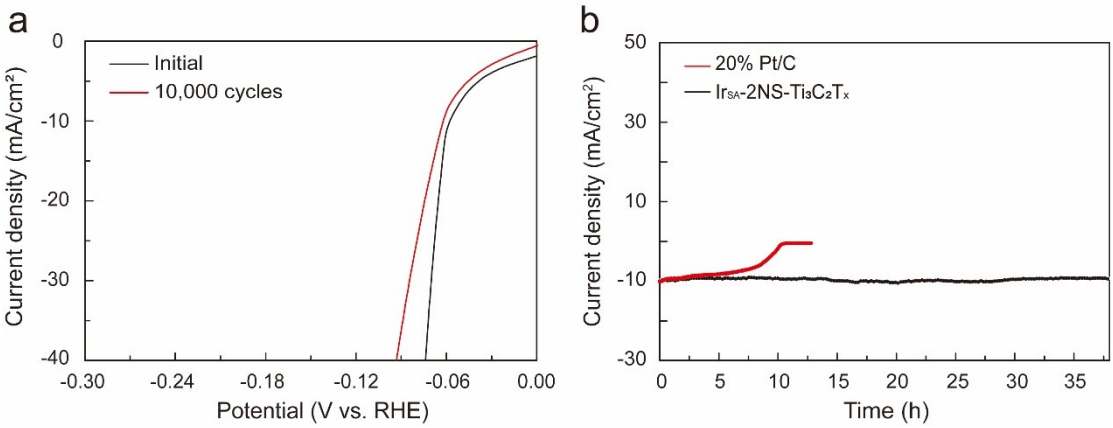

Figure S15. (a) LSV curves before and after 10,000 CV cycles for Ir_{SA}-2NS-$Ti_3C_2T_x$ in acidic condition. **(b)** Durability test of Ir_{SA}-2NS-$Ti_3C_2T_x$ electrocatalyst in 0.5 M H_2SO_4.

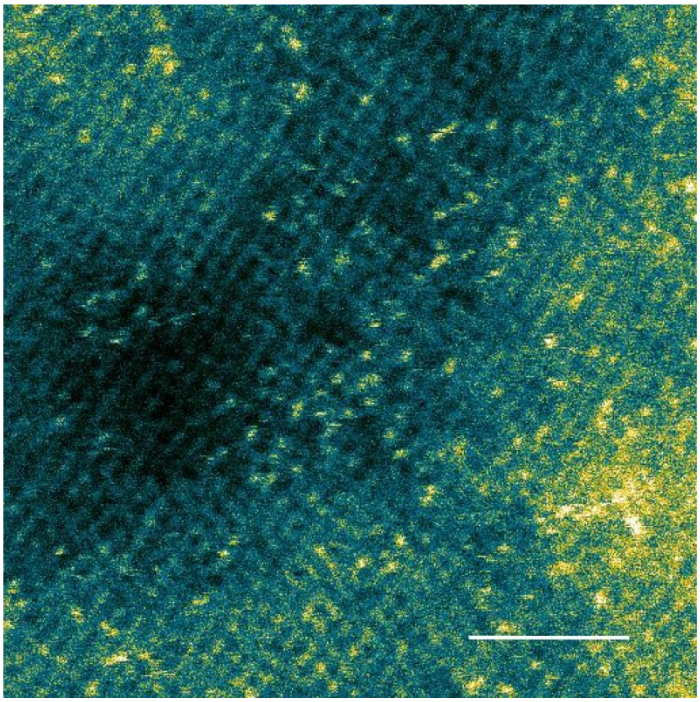

Figure S16. Magnified HAADF-STEM image of Ir_{SA}-2NS-$Ti_3C_2T_x$, after HER test. Scale bar: 2 nm.

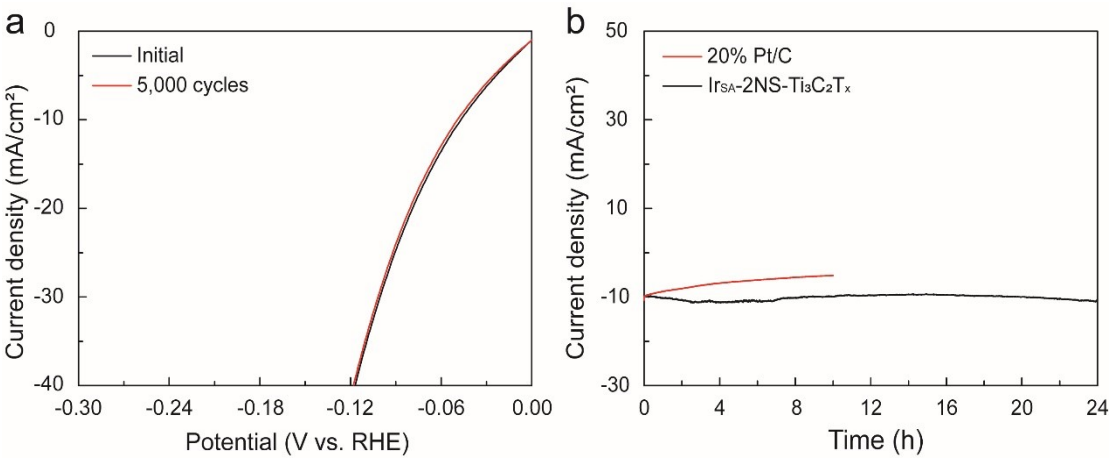

Figure S17. (a) LSV curves before and after 5,000 CV cycles for Ir_{SA}-2NS-$Ti_3C_2T_x$ in alkaline condition. (b) Durability test of Ir_{SA}-2NS-$Ti_3C_2T_x$ electrocatalyst in 1 M KOH.

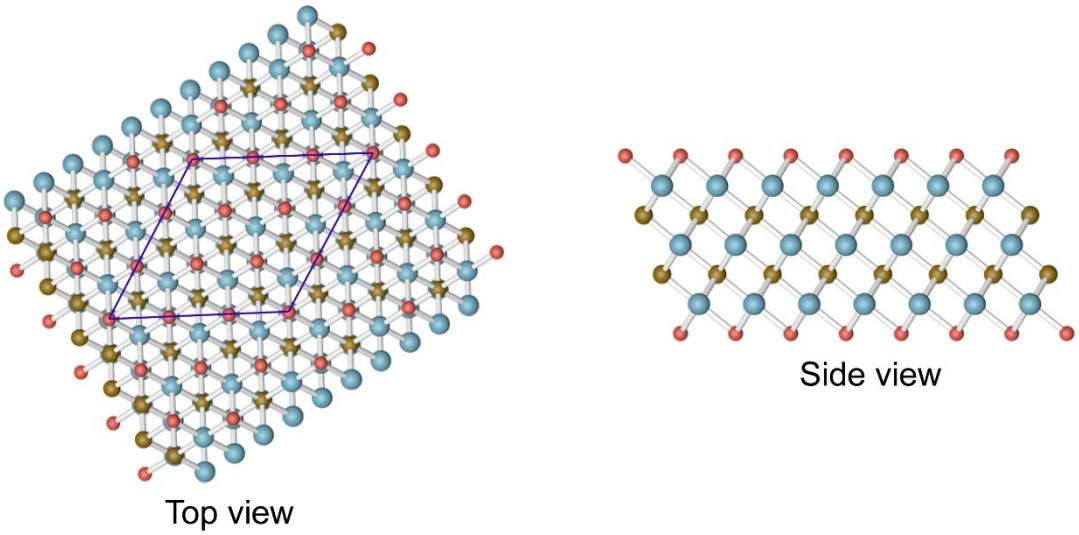

Figure S18. Top view and side view of the $Ti_3C_2T_x$ atomic model (Blue: Ti; red: O; brown: C).

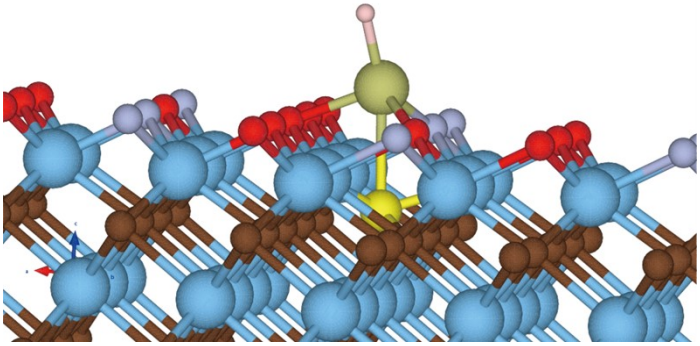

Figure S19. Atomic model of the Ir_{SA}-2NS-$Ti_3C_2T_x$ (Blue: Ti; red: O; brown: C; yellow: S; light purple: N; light olive green: Ir; pink: H).

Table S1. The S atomic ratio data of Ir_{SA}-1NS-$Ti_3C_2T_x$, Ir_{SA}-2NS-$Ti_3C_2T_x$ and Ir_{SA}-3NS-$Ti_3C_2T_x$ from XPS result.

	Ir_{SA}-1NS-$Ti_3C_2T_x$	Ir_{SA}-2NS-$Ti_3C_2T_x$	Ir_{SA}-3NS-$Ti_3C_2T_x$
Atomic %	0.46	0.49	0.47

Table S2. The Ir-N content of Ir_{SA}-NS-$Ti_3C_2T_x$ calculated from XPS result.

Ir_{SA}-1NS-$Ti_3C_2T_x$

Peak	Position (eV)	Area
Ti-N	396.050	6000.000
pyridinic-N	396.990	7740.593
N-Ti-O	398.610	3051.462
Ir-N	400.200	1450.466

Ir_{SA}-2NS-$Ti_3C_2T_x$

Peak	Position (eV)	Area
Ti-N	396.100	4751.382
pyridinic-N	397.500	6986.950
N-Ti-O	398.610	1622.417
Ir-N	400.200	1493.673

Ir_{SA}-3NS-$Ti_3C_2T_x$

Peak	Position (eV)	Area
Ti-N	396.310	2901.936
pyridinic-N	396.810	9163.916
N-Ti-O	398.610	3979.977
Ir-N	400.200	3152.189

Table S3. Structural parameters extracted from the Ir L3-edge EXAFS fitting of Ir_{SA}-2NS-$Ti_3C_2T_x$

Catalysts	**Scattering pair**	***CN***	***R* (Å)**	**σ^2 (10^{-3} Å²)**	**ΔE_0 (eV)**	***R*-factor**
Ir_{SA}-2NS-$Ti_3C_2T_x$	Ir-N(O)	2.8	2.01	3.25	5.87	0.01
	Ir-S	1.2	2.65	5.02	4.96	0.01

Note: *CN* represents the coordination number; *R* represents the interatomic distance; σ^2 represents the Debye-Waller factor; ΔE_0 represents the edge-energy shift.

Table S4. Catalytic performances in acid media of electrocatalysts prepared in this work compared with previously reported MXene-based catalysts in other literatures.

Catalyst	η @ 10 mA/cm² (mV)	Tafel slope (mV/dec)	Reference
Ir_{SA}-2NS-$Ti_3C_2T_x$	58	25.1	This work
Ir_{SA}-NS-$Ti_3C_2T_x$	109	73.8	This work
Ir_{SA}-3NS-$Ti_3C_2T_x$	87	50.5	This work
$Pt_{3.21}Ni@Ti_3C_2$	18.55	13.3	[1]
Pt/Ti_3C_2-550	32.7	32.3	[2]
Ru@B-$Ti_3C_2T_x$	62.9	100	[3]
Ru_{SA}-N-S-$Ti_3C_2T_x$	76	90	[4]
$Mo_2TiC_2T_x$–Pt_{SA}	30	30	[5]
MoS_2/Ti_3C_2@C	135	45	[6]
Mo_2C/$Ti_3C_2T_x$@NC	53	40	[7]
Mo_2CT_x MXene	189	70	[8]
MoS_2/$Ti_3C_2T_x$	152	70	[9]
N-Ti_2CT_x	215	67	[10]

Ru_{SA}–N-$Ti_3C_2T_x$	23	35	[11]
D-Mo_2TiC_2/Ni	78	56.7	[12]
S-M-5Pt	62	78	[13]
$TiOF_2$@$Ti_3C_2T_x$	103	56.2	[14]

Table S5. Catalytic performances in acid media of electrocatalysts prepared in this compared work with previously reported catalysts in other literatures.

Catalyst	η @ 10 mA/cm^2 (mV)	Tafel slope (mV/dec)	Reference
Ir_{SA}-2NS-$Ti_3C_2T_x$	58	25.1	This work
Pt-MoS_2（0.1M H_2SO_4）	60	96	[15]
Mo_2C@NG/CNT	160	65	[16]
Ru/g-C_3N_4-C-TiO_2	112	83	[17]
MoS_2@Mo-S-C_3N_4	193	65	[18]
Pt@PCM	105	65.3	[19]
a-$RuTe_2$ PNRs	33	35	[20]
Pt-SAs/WS_2	32	28	[21]
Pt_1/OLC	38	36	[22]
Pt SA/mWO_3−x	47	45	[23]
Pt-Ru dimer	50	28.9	[24]
Pd NPs-Bis 24h	59.6	30	[25]
IrNiTa/Si	99	35	[26]
IrCo@NC-850	50	25	[27]

Table S6. Catalytic performances in alkaline electrolyte of prepared electrocatalysts compared with previously reported catalysts in other literatures.

Catalyst	η @ 10 mA/cm^2 (mV)	Tafel slope (mV/dec)	Reference
Ir_{SA}-2NS-$Ti_3C_2T_x$	40.8	50.5	This work
Ir-N-$Ti_3C_2T_x$	274.6	235.1	
$Pt_{3.21}Ni$@Ti_3C_2 (0.1M KOH)	55@5	37	[1]
$Ni_{0.9}Co_{0.1}$@NTM	43.4	116	[28]
Ni@NTM	177.4	185	
$Ni_{0.7}Fe_{0.3}PS_3$@$Ti_3C_2T_x$ MXene	196	N.A.	[29]
Ti_3C_2@mNiCoP	127	103	[30]
Ti_3C_2@$NiCO_4$	248	161	
NiS_2/V-MXene	179	85	[31]
NiS_2/Ti-MXene	210	100	
CoP@Ti_3C_2-MXene	243	66	[32]
BP QDs/$Ti_3C_2T_x$ MXene	190	83	[33]
VOOH/$Ti_3C_2T_x$ MXene	100	81.8	[34]

Reference

[1] Y. Jiang, X. Wu, Y. Yan, S. Luo, X. Li, J. Huang, H. Zhang, D. Yang, *Small* 2019, **15**, 1805474.

[2] Z. Li, Z. Qi, S. Wang, T. Ma, L. Zhou, Z. Wu, X. Luan, F.Y. Lin, M. Chen, J.T. Miller, H. Xin, W. Huang, Y. Wu, *Nano Lett.* 2019, **19**, 5102-5108.

[3] M. Bat-Erdene, M. Batmunkh, B. Sainbileg, M. Hayashi, A.S.R. Bati, J. Qin, H. Zhao, Y.L. Zhong, J.G. Shapter, *Small* 2021, **17**, 2102218.

[4] V. Ramalingam, P. Varadhan, H.C. Fu, H. Kim, D. Zhang, S. Chen, L. Song, D. Ma, Y. Wang, H.N. Alshareef, J.H. He, *Adv. Mater.* 2019, **31**, 1903841.

[5] J. Zhang, Y. Zhao, X. Guo, C. Chen, C.-L. Dong, R.-S. Liu, C.-P. Han, Y. Li, Y. Gogotsi, G. Wang, *Nat. Catal.* 2018, **1**, 985-992.

[6] X. Wu, Z. Wang, M. Yu, L. Xiu, J. Qiu, *Adv. Mater.* 2017, **29**, 1607017.

[7] H. Wang, Y. Lin, S. Liu, J. Li, L. Bu, J. Chen, X. Xiao, J.-H. Choi, L. Gao, J.-M. Lee, *J. Mater. Chem. A* 2020, **8**, 7109-7116.

[8] Z.W. Seh, K.D. Fredrickson, B. Anasori, J. Kibsgaard, A.L. Strickler, M.R. Lukatskaya, Y. Gogotsi, T.F. Jaramillo, A. Vojvodic, *ACS Energy Lett.* 2016, **1**, 589-594.

[9] J. Liu, Y. Liu, D. Xu, Y. Zhu, W. Peng, Y. Li, F. Zhang, X. Fan, *Appl. Catal. B Environ.* 2019, **241**, 89-94.

[10] Y. Yoon, A.P. Tiwari, M. Lee, M. Choi, W. Song, J. Im, T. Zyung, H.-K. Jung, S.S. Lee, S. Jeon, K.-S. An, *J. Mater. Chem. A* 2018, **6**, 20869-20877.

[11] H. Liu, Z. Hu, Q. Liu, P. Sun, Y. Wang, S. Chou, Z. Hu, Z. Zhang, *J. Mater.*

Chem. A 2020, **8**, 24710-24717.

[12] Y. Zhu, G. Xu, W. Song, Y. Zhao, Z. He, Z. Miao, *Ceram. Int.* 2021, **47**, 30005-30011.

[13] C. Cui, R. Cheng, H. Zhang, C. Zhang, Y. Ma, C. Shi, B. Fan, H. Wang, X. Wang, *Adv. Funct. Mater.* 2020, **30**, 2000693.

[14] Z. Wang, K. Yu, Y. Feng, R. Qi, J. Ren, Z. Zhu, *Appl. Surf. Sci.* 2019, **496**, 143729.

[15] J. Deng, H. Li, J. Xiao, Y. Tu, D. Deng, H. Yang, H. Tian, J. Li, P. Ren, X. Bao, *Energy Environ. Sci.* 2015, **8**, 1594-1601.

[16] C. Yang, K. Shen, R. Zhao, H. Xiang, J. Wu, W. Zhong, Q. Zhang, X. Li, N. Yang, *Adv. Funct. Mater.* 2021, **32**, 2108167.

[17] Z. Li, Y. Yang, S. Wang, L. Gu, S. Shao, *ACS Appl. Mater. Interfaces* 2021, **13**, 46608-46619.

[18] B. Zhang, J. Li, Q. Song, X. Xu, W. Hou, H. Liu, *Inorg. Chem.* 2021, **60**, 2604-2613.

[19] P.A. Huabin Zhang, Wei Zhou, Bu Yuan Guan, Peng Zhang, Juncai Dong, Xiong Wen (David) Lou, *Sci. Adv.* 2018, **4**, eaao6657.

[20] J. Wang, L. Han, B. Huang, Q. Shao, H.L. Xin, X. Huang, *Nat. Commun.* 2019, **10**, 5692.

[21] Y. Shi, Z.R. Ma, Y.Y. Xiao, Y.C. Yin, W.M. Huang, Z.C. Huang, Y.Z. Zheng, F.Y. Mu, R. Huang, G.Y. Shi, Y.Y. Sun, X.H. Xia, W. Chen, *Nat. Commun.* 2021, **12**, 3021.

[22] D. Liu, X. Li, S. Chen, H. Yan, C. Wang, C. Wu, Y.A. Haleem, S. Duan, J. Lu, B. Ge, P.M. Ajayan, Y. Luo, J. Jiang, L. Song, *Nat. Energy* 2019, **4**, 512-518.

[23] J. Park, S. Lee, H.E. Kim, A. Cho, S. Kim, Y. Ye, J.W. Han, H. Lee, J.H. Jang, J. Lee, *Angew. Chem. Int. Ed.* 2019, **58**, 16038.

[24] L. Zhang, R. Si, H. Liu, N. Chen, Q. Wang, K. Adair, Z. Wang, J. Chen, Z. Song, J. Li, M.N. Banis, R. Li, T.K. Sham, M. Gu, L.M. Liu, G.A. Botton, X. Sun, *Nat. Commun.* 2019, **10**, 4936.

[25] H. Cheng, N. Yang, G. Liu, Y. Ge, J. Huang, Q. Yun, Y. Du, C.J. Sun, B. Chen, J. Liu, H. Zhang, *Adv. Mater.* 2020, **32**, 1902964.

[26] Z.J. Wang, M.X. Li, J.H. Yu, X.B. Ge, Y.H. Liu, W.H. Wang, *Adv. Mater.* 2020, **32**, 1906384.

[27] Y.Q. Zhou, L. Zhang, H.L. Suo, W. Hua, S. Indris, Y. Lei, W.H. Lai, Y.X. Wang, Z. Hu, H.K. Liu, S.L. Chou, S.X. Dou, *Adv. Funct. Mater.* 2021, **31**, 2101797.

[28] C.F. Du, X. Sun, H. Yu, Q. Liang, K.N. Dinh, Y. Zheng, Y. Luo, Z. Wang, Q. Yan, *Adv. Sci.* 2019, **6**, 1900116.

[29] C.-F. Du, K.N. Dinh, Q. Liang, Y. Zheng, Y. Luo, J. Zhang, Q. Yan, *Adv. Energy Mater.* 2018, **8**, 1801127.

[30] Q. Yue, J. Sun, S. Chen, Y. Zhou, H. Li, Y. Chen, R. Zhang, G. Wei, Y. Kang, *ACS Appl. Mater. Interfaces* 2020, **12**, 18570-18577.

[31] P. Kuang, M. He, B. Zhu, J. Yu, K. Fan, M. Jaroniec, *J. Catal.* 2019, **375**, 8-20.

[32] L. Xiu, Z. Wang, M. Yu, X. Wu, J. Qiu, *ACS Nano* 2018, **12**, 8017-8028.

[33] X.-D. Zhu, Y. Xie, Y.-T. Liu, *J. Mater. Chem. A* 2018, **6**, 21255-21260.

[34] L. Yan, X. Chen, X. Liu, L. Chen, B. Zhang, *J. Mater. Chem. A* 2020, **8**, 23637-23644.